Hindawi
Advances in Mathematical Physics
Volume 2022, Article ID 9743699, 14 pages
https://doi.org/10.1155/2022/9743699

Research Article

A High Accuracy Local One-Dimensional Explicit Compact Scheme for the 2D Acoustic Wave Equation

Mengling Wu,[1] Yunzhi Jiang,[2] and Yongbin Ge[1]

[1]*Institute of Applied Mathematics and Mechanics, Ningxia University, Yinchuan 750021, China*
[2]*Basic Courses Teaching and Research Department, Yingkou Institute of Technology, Yingkou 115100, China*

Correspondence should be addressed to Yongbin Ge; gybnxu@yeah.net

Received 16 March 2022; Accepted 3 May 2022; Published 26 May 2022

Academic Editor: Ivan Giorgio

In this paper, we develop a highly accurate and efficient finite difference scheme for solving the two-dimensional (2D) wave equation. Based on the local one-dimensional (LOD) method and Padé difference approximation, a fourth-order accuracy explicit compact difference scheme is proposed. Then, the Fourier analysis method is used to analyze the stability of the scheme, which shows that the new scheme is conditionally stable and the Courant-Friedrichs-Lewy (CFL) condition is superior to most existing methods of equivalent order of accuracy in the literature. Finally, numerical experiments demonstrate the high accuracy, stability, and efficiency of the proposed method.

1. Introduction

Wave equation is mainly used to describe various wave phenomena in nature, such as sound wave, light wave, and water wave. Due to complex physical background, it is very difficult to obtain the exact solutions of practical problems. Therefore, researches on numerical solutions of initial value (or initial-boundary value) problems for wave equation have extremely important theoretical value and practical significance.

The finite difference method is one of the most important and popular methods for solving the wave equation. It has many advantages, such as it is easy to be implemented, has low memory requirement, and has a high computing speed [1–8]. The second-order central difference scheme is the most commonly used, but when the number of spatial sampling points per wavelength is too small, the method has serious dispersion. In order to effectively suppress numerical dispersion, Yang et al. [9] proposed a local interpolation strategy based on the Runge-Kutta method. Later, for solving large-scale problems, Yang et al. [10] proposed an approximate analytic central difference method. However, both methods are conditionally stable; their maximum values of CFL conditions are 0.5080 [9] and 0.8440 [10], respectively. Most of the existing schemes with fourth-order accuracy in both space and time have very strict stability conditions. For instance, Wang et al. [11] developed a new finite difference stencil where the range of the CFL number is 0.7071. Feo et al. [12] combined novel tensor mimetic discretizations in space and a leapfrog approximation in time to produce an explicit scheme; the range of the CFL number is 0.8660. In addition, many implicit finite difference schemes are also used to solve the 2D wave equations [13–16]. For instance, Wang et al. [13] introduced two efficient fourth-order implicit time-space-domain finite difference schemes by using linear and nonlinear optimization methods. The high-order compact (HOC), compact Padé difference, and noncompact Padé difference implicit schemes were proposed in Ref. [14], all of which have a truncation error of $O(\tau^4 + \tau^2 h^2 + h^4)$. Since these implicit difference methods require iterations at each time step, this greatly increases the computational cost. In order to improve the computational efficiency, a combination of the finite difference method and splitting method is used by many researchers [17, 18]. Two types of classical splitting methods are the alternating direction implicit (ADI) method and the LOD method. Both of these methods simplify the multidimensional problems into a series of one-dimensional (1D)

problems that form the tridiagonal systems and are easy to be solved. The ADI method was originally introduced by Peaceman and Rachford [19] to solve parabolic and elliptic equations. It was also used to solve hyperbolic equations [20, 21]. Up to now, many ADI methods have been studied to solve the wave equations [22–26]. For instance, Das et al. [22] and Liao et al. [23] used a combination of ADI and the Padé approximation to derive a difference scheme with fourth-order accuracy and low numerical dispersion. Their maximum values of CFL conditions are 0.7657 [22] and 0.7321 [23], respectively. Qin [24] constructed a compact Douglas scheme based on the ADI method, which has fourth-order accuracy in space, but only second-order accuracy in time.

On the other hand, the LOD method was originally introduced by Samarskii [27] for solving the 2D hyperbolic equations. The LOD technique has been proven to be very useful in reducing computer memory and computational cost and improving stability [28, 29]. We notice that many researchers mainly study the homogeneous wave equation. For instance, Yun et al. [30] applied a new fourth-order accuracy optimal nearly analytic splitting method to solve the 2D acoustic wave equation based on the LOD method. Sim et al. [31] proposed a nearly analytic symplectic partitioned Runge-Kutta method based on the LOD technique, which has second-order temporal accuracy and fourth-order spatial accuracy. Very recently, Zhang [29] considered the nonhomogeneous wave equation and set an unknown parameter θ in front of the source term. Then, the value of θ was calculated by solving a series of large matrices, so as to obtain an implicit scheme with fourth-order accuracy in both time and space. This method increases computational complexity and reduces computational efficiency. Therefore, in this paper, we are aiming at developing an explicit compact difference method for solving the 2D nonhomogeneous wave equation based on the LOD method. The merits of the present method include high-order accuracy, better stability, and easy treatment for the nonhomogeneous term.

The structure of this paper is arranged as follows. In Section 2, the derivation of the new explicit HOC difference scheme based on the LOD method is given and the corresponding numerical algorithm is introduced. In Section 3, the stability of the new scheme is analyzed. In Section 4, the numerical examples are employed to verify our theoretical analysis results. Finally, the conclusion is given in Section 5.

2. Derivation of the New Scheme

The 2D wave equation with variable wave velocity is as follows:

$$\frac{\partial^2 u}{\partial t^2} = v^2(x,y)\left(\frac{\partial^2 u}{\partial x^2} + \frac{\partial^2 u}{\partial y^2}\right) + f(x,y,t), (x,y,t) \in \Omega \times (0,T], \tag{1}$$

with the initial conditions

$$u(x,y,0) = \varphi(x,y), \frac{\partial u(x,y,0)}{\partial t} = \psi(x,y), (x,y) \in \Omega, \tag{2}$$

and the Dirichlet boundary conditions

$$u(x,y,t) = g(x,y,t), (x,y,t) \in \partial\Omega \times (0,T], \tag{3}$$

where $u(x,y,t)$ represents pressure and $v(x,y)$ is the wave velocity. $f(x,y,t)$ is the source term. $\varphi(x,y)$, $\psi(x,y)$, and $g(x,y,t)$ are known smooth functions. $\Omega = [\alpha,\beta] \times [\alpha,\beta]$, $\Omega \subset R^2$, and $\partial\Omega$ represent the boundary of Ω. α, β are constants, and $\alpha < \beta$. $(0,T]$ is the time region.

$[\alpha,\beta]$ is divided into N subintervals by equidistant grid, and the space step length is represented by $h = (\beta - \alpha)/N$. $(0,T]$ is also equally divided into M subintervals, and the time step length is $\tau = T/M$. We use (x_i, y_j, t_n) which represents the mesh point, $x_i = \alpha + ih, y_j = \alpha + jh, i,j = 0,1,\cdots N, t_n = n\tau, n = 0,1,\cdots M$.

The LOD method is used to ideally split the 2D wave equation (1) into two 1D wave equations (27) as follows:

$$\frac{1}{2}\frac{\partial^2 u}{\partial t^2} = v^2(x,y)\frac{\partial^2 u}{\partial x^2} + \frac{1}{2}f(x,y,t), \tag{4}$$

$$\frac{1}{2}\frac{\partial^2 u}{\partial t^2} = v^2(x,y)\frac{\partial^2 u}{\partial y^2} + \frac{1}{2}f(x,y,t). \tag{5}$$

To advance the solution from $u(x_i, y_j, t_n)$ to $u(x_i, y_j, t_{n+1})$, we assume that Equation (4) holds from $u(x_i, y_j, t_n)$ to $u(x_i, y_j, t_{n+1/2})$ and Equation (5) holds from $u(x_i, y_j, t_{n+1/2})$ to $u(x_i, y_j, t_{n+1})$.

Firstly, we consider Equation (4) at the grid point (x_i, y_j, t_n), i.e.,

$$\frac{1}{2}\left(\frac{\partial^2 u}{\partial t^2}\right)_{i,j}^n = v_{i,j}^2\left(\frac{\partial^2 u}{\partial x^2}\right)_{i,j}^n + \frac{1}{2}f_{i,j}^n. \tag{6}$$

For the time second derivative $\partial^2 u/\partial t^2$ on the left side of Equation (6), we adopt the following expression:

$$\left(\frac{\partial^2 u}{\partial t^2}\right)_{i,j}^n = 4\frac{u_{i,j}^{n+1/2} - 2u_{i,j}^n + u_{i,j}^{n-1/2}}{\tau^2} - \frac{\tau^2}{48}\left(\frac{\partial^4 u}{\partial t^4}\right)_{i,j}^n + O(\tau^4). \tag{7}$$

According to the Equation (4), we have

$$\frac{\partial^4 u}{\partial t^4} = \frac{\partial^2}{\partial t^2}\left(\frac{\partial^2 u}{\partial t^2}\right) = 2v^2\frac{\partial^2}{\partial x^2}\left(\frac{\partial^2 u}{\partial t^2}\right) + \frac{\partial^2 f}{\partial t^2}. \tag{8}$$

We define the central difference operator for the spatial second derivative as follows:

$$\delta_x^2 u_{i,j}^n = \frac{u_{i+1,j}^n - 2u_{i,j}^n + u_{i-1,j}^n}{h^2}. \tag{9}$$

Substituting Equations (8) and (9) into Equation (7), we obtain

$$\left(\frac{\partial^2 u}{\partial t^2}\right)_{i,j}^{n} = 4\frac{u_{i,j}^{n+1/2} - 2u_{i,j}^{n} + u_{i,j}^{n-1/2}}{\tau^2} - \frac{v_{i,j}^2\tau^2}{24}\frac{\partial^2}{\partial x^2}\left(\frac{\partial^2 u}{\partial t^2}\right)_{i,j}^{n} - \frac{\tau^2}{48}\left(\frac{\partial^2 f}{\partial t^2}\right)_{i,j}^{n} + O\left(\tau^4\right) = 4\frac{u_{i,j}^{n+1/2} - 2u_{i,j}^{n} + u_{i,j}^{n-1/2}}{\tau^2} - \frac{v_{i,j}^2\tau^2}{24}\delta_x^2\left(\frac{\partial^2 u}{\partial t^2}\right)_{i,j}^{n} - \frac{\tau^2}{48}\left(\frac{\partial^2 f}{\partial t^2}\right)_{i,j}^{n} + O\left(\tau^4 + \tau^2 h^2\right) = 4\frac{u_{i,j}^{n+1/2} - 2u_{i,j}^{n} + u_{i,j}^{n-1/2}}{\tau^2} - \frac{v_{i,j}^2\tau^2}{24h^2}\left[\left(\frac{\partial^2 u}{\partial t^2}\right)_{i+1,j}^{n} + \left(\frac{\partial^2 u}{\partial t^2}\right)_{i-1,j}^{n}\right] + \frac{v_{i,j}^2\tau^2}{12h^2}\left(\frac{\partial^2 u}{\partial t^2}\right)_{i,j}^{n} - \frac{\tau^2}{48}\left(\frac{\partial^2 f}{\partial t^2}\right)_{i,j}^{n} + O\left(\tau^4 + \tau^2 h^2\right). \tag{10}$$

It can be rewritten as

$$u_{i,j}^{n+1/2} = 2u_{i,j}^{n} - u_{i,j}^{n-1/2} + \frac{v_{i,j}^2\tau^4}{96h^2}\left[\left(\frac{\partial^2 u}{\partial t^2}\right)_{i+1,j}^{n} - 2\left(\frac{\partial^2 u}{\partial t^2}\right)_{i,j}^{n} + \left(\frac{\partial^2 u}{\partial t^2}\right)_{i-1,j}^{n}\right] + \frac{\tau^2}{4}\left(\frac{\partial^2 u}{\partial t^2}\right)_{i,j}^{n} + \frac{\tau^4}{192}\left(\frac{\partial^2 f}{\partial t^2}\right)_{i,j}^{n} + O\left(\tau^4 + \tau^2 h^2\right). \tag{11}$$

Defining the grid ratio $\lambda = \tau/h$, substituting Equation (4) into Equation (11), and omitting the truncation error term, we obtain

$$u_{i,j}^{n+1/2} = 2u_{i,j}^{n} - u_{i,j}^{n-1/2} + \frac{v_{i,j}^2\tau^2\lambda^2}{48}\left[v_{i+1,j}^2\left(\frac{\partial^2 u}{\partial x^2}\right)_{i+1,j}^{n} + v_{i-1,j}^2\left(\frac{\partial^2 u}{\partial x^2}\right)_{i-1,j}^{n}\right] + \left(\frac{v_{i,j}^2\tau^2}{2} - \frac{v_{i,j}^4\tau^2\lambda^2}{24}\right)\left(\frac{\partial^2 u}{\partial x^2}\right)_{i,j}^{n} + \frac{v_{i,j}^2\tau^2\lambda^2}{96}\left(f_{i+1,j}^{n} + f_{i-1,j}^{n}\right) + \left(\frac{\tau^2}{4} - \frac{v_{i,j}^2\tau^2\lambda^2}{48}\right)f_{i,j}^{n} + \frac{\tau^4}{192}\left(\frac{\partial^2 f}{\partial t^2}\right)_{i,j}^{n}. \tag{12}$$

The function f and its derivative $\partial^2 f/\partial t^2$ are known at each grid point. Next, we use the fourth-order Padé scheme given in Ref. [32] to calculate the unknown term $(\partial^2 u/\partial x^2)^n$ in Equation (12) as follows:

$$\left(\frac{\partial^2 u}{\partial x^2}\right)_{i+1,j}^{n} + 10\left(\frac{\partial^2 u}{\partial x^2}\right)_{i,j}^{n} + \left(\frac{\partial^2 u}{\partial x^2}\right)_{i-1,j}^{n} = 12\frac{u_{i+1,j}^{n} - 2u_{i,j}^{n} + u_{i-1,j}^{n}}{h^2} + O\left(h^4\right), \quad i = 1, 2, \cdots, N-1, j = 0, 1, \cdots N, \tag{13}$$

in which the nodes of the $(\partial^2 u/\partial x^2)_{i,j}^{n}$ on the boundaries can be obtained by using Equations (3) and (6):

$$\left(\frac{\partial^2 u}{\partial x^2}\right)_{0,j}^{n} = \frac{1}{2v_{0,j}^2}\left(\frac{\partial^2 u}{\partial t^2} - f\right)_{0,j}^{n} = \frac{1}{2v_{0,j}^2}\left(\frac{\partial^2 g}{\partial t^2} - f\right)_{0,j}^{n}, \quad j = 0, 1, \cdots N, \tag{14}$$

$$\left(\frac{\partial^2 u}{\partial x^2}\right)_{N,j}^{n} = \frac{1}{2v_{N,j}^2}\left(\frac{\partial^2 u}{\partial t^2} - f\right)_{N,j}^{n} = \frac{1}{2v_{N,j}^2}\left(\frac{\partial^2 g}{\partial t^2} - f\right)_{N,j}^{n}, \quad j = 0, 1, \cdots N. \tag{15}$$

Then, we consider Equation (5) at the grid point $(x_i, y_j, t_{n+1/2})$, i.e.,

$$\frac{1}{2}\left(\frac{\partial^2 u}{\partial t^2}\right)_{i,j}^{n+1/2} = v_{i,j}^2\left(\frac{\partial^2 u}{\partial y^2}\right)_{i,j}^{n+1/2} + \frac{1}{2}f_{i,j}^{n+1/2}. \tag{16}$$

Using a similar treatment process as for Equation (6), omitting the truncation error terms, we can obtain

$$u_{i,j}^{n+1} = 2u_{i,j}^{n+1/2} - u_{i,j}^{n} + \frac{v_{i,j}^2\tau^2\lambda^2}{48}\left[v_{i,j+1}^2\left(\frac{\partial^2 u}{\partial y^2}\right)_{i,j+1}^{n+1/2} + v_{i,j-1}^2\left(\frac{\partial^2 u}{\partial y^2}\right)_{i,j-1}^{n+1/2}\right] + \left(\frac{v_{i,j}^2\tau^2}{2} - \frac{v_{i,j}^4\tau^2\lambda^2}{24}\right)\left(\frac{\partial^2 u}{\partial y^2}\right)_{i,j}^{n+1/2} + \frac{v_{i,j}^2\tau^2\lambda^2}{96}\left(f_{i,j+1}^{n+1/2} + f_{i,j-1}^{n+1/2}\right) + \left(\frac{\tau^2}{4} - \frac{v_{i,j}^2\tau^2\lambda^2}{48}\right)f_{i,j}^{n+1/2} + \frac{\tau^4}{192}\left(\frac{\partial^2 f}{\partial t^2}\right)_{i,j}^{n+1/2}. \tag{17}$$

The internal nodes of the $(\partial^2 u/\partial y^2)_{i,j}^{n+1/2}$ can also be computed by the fourth-order Padé scheme [32].

$$\left(\frac{\partial^2 u}{\partial y^2}\right)_{i,j+1}^{n+1/2} + 10\left(\frac{\partial^2 u}{\partial y^2}\right)_{i,j}^{n+1/2} + \left(\frac{\partial^2 u}{\partial y^2}\right)_{i,j-1}^{n+1/2} = 12\frac{u_{i,j+1}^{n+1/2} - 2u_{i,j}^{n+1/2} + u_{i,j-1}^{n+1/2}}{h^2} + O\left(h^4\right), \quad i = 0, 1, \cdots N, j = 1, 2, \cdots, N-1, \tag{18}$$

in which, the nodes of the $(\partial^2 u/\partial y^2)_{i,j}^{n+1/2}$ on the boundaries can be obtained by using Equations (3) and (16):

$$\left(\frac{\partial^2 u}{\partial y^2}\right)_{i,0}^{n+1/2} = \frac{1}{2v_{i,0}^2}\left(\frac{\partial^2 u}{\partial t^2} - f\right)_{i,0}^{n+1/2} = \frac{1}{2v_{i,0}^2}\left(\frac{\partial^2 g}{\partial t^2} - f\right)_{i,0}^{n+1/2}, \quad i = 0, 1, \cdots N, \tag{19}$$

$$\left(\frac{\partial^2 u}{\partial y^2}\right)_{i,N}^{n+1/2} = \frac{1}{2v_{i,N}^2}\left(\frac{\partial^2 u}{\partial t^2} - f\right)_{i,N}^{n+1/2} = \frac{1}{2v_{i,N}^2}\left(\frac{\partial^2 g}{\partial t^2} - f\right)_{i,N}^{n+1/2}, \quad i = 0, 1, \cdots N. \tag{20}$$

Applying Equations (12)–(20), we can complete the entire calculation from $u(x_i, y_j, t_n)$ to $u(x_i, y_j, t_{n+1})$ for Equation (1). The scheme is an explicit HOC difference scheme based on the LOD method, which can be denoted as the EHOC-LOD scheme. According to the derivation process, we know that the EHOC-LOD scheme is a four-level scheme with fourth-order accuracy in both time and space. Therefore, two start-up time steps need to be calculated at $t = \tau/2$ and $t = \tau$. To approximate the start-up time steps $u_{i,j}^{1/2}$ and $u_{i,j}^{1}$, using Taylor's expansions, we have

$$u_{i,j}^{1/2} = u_{i,j}^{0} + \frac{\tau}{2}\left(\frac{\partial u}{\partial t}\right)_{i,j}^{0} + \frac{\tau^2}{8}\left(\frac{\partial^2 u}{\partial t^2}\right)_{i,j}^{0} + \frac{\tau^3}{48}\left(\frac{\partial^3 u}{\partial t^3}\right)_{i,j}^{0} + \frac{\tau^4}{384}\left(\frac{\partial^4 u}{\partial t^4}\right)_{i,j}^{0} + O\left(\tau^5\right), \tag{21}$$

$$u_{i,j}^{1} = u_{i,j}^{0} + \tau\left(\frac{\partial u}{\partial t}\right)_{i,j}^{0} + \frac{\tau^2}{2}\left(\frac{\partial^2 u}{\partial t^2}\right)_{i,j}^{0} + \frac{\tau^3}{6}\left(\frac{\partial^3 u}{\partial t^3}\right)_{i,j}^{0} + \frac{\tau^4}{24}\left(\frac{\partial^4 u}{\partial t^4}\right)_{i,j}^{0} + O\left(\tau^5\right). \tag{22}$$

For simplicity, we denote the time-independent functions as the following notations:

$$\frac{\partial \varsigma}{\partial x} = \varsigma_x,\ \frac{\partial \varsigma}{\partial y} = \varsigma_y,\ \frac{\partial^2 \varsigma}{\partial x^2} = \varsigma_{xx},\ \frac{\partial^2 \varsigma}{\partial y^2} = \varsigma_{yy},$$

$$\frac{\partial^3 \varsigma}{\partial x^3} = \varsigma_{xxx},\ \frac{\partial^3 \varsigma}{\partial x \partial y^2} = \varsigma_{xyy},\ \frac{\partial^3 \varsigma}{\partial y^3} = \varsigma_{yyy},\ \frac{\partial^3 \varsigma}{\partial y \partial x^2} = \varsigma_{xxy},$$

$$\frac{\partial^4 \varsigma}{\partial x^4} = \varsigma_{xxxx},\ \frac{\partial^4 \varsigma}{\partial y^4} = \varsigma_{yyyy},\ \frac{\partial^4 \varsigma}{\partial x^2 \partial y^2} = \varsigma_{xxyy}, \tag{23}$$

in which ς can represent φ, ψ, v^2, etc.

By using Equations (1) and (2), we can get

$$\left(\frac{\partial^2 u}{\partial t^2}\right)_{i,j}^{0} = v_{i,j}^2\left(\frac{\partial^2 u}{\partial x^2} + \frac{\partial^2 u}{\partial y^2}\right)_{i,j}^{0} + f_{i,j}^{0} = v_{i,j}^2\left(\varphi_{xx} + \varphi_{yy}\right)_{i,j} + f_{i,j}^{0}, \tag{24}$$

$$\left(\frac{\partial^3 u}{\partial t^3}\right)_{i,j}^{0} = \frac{\partial}{\partial t}\left(\frac{\partial^2 u}{\partial t^2}\right)_{i,j}^{0} = v_{i,j}^2\left[\left(\frac{\partial^2}{\partial x^2} + \frac{\partial^2}{\partial y^2}\right)\left(\frac{\partial u}{\partial t}\right)_{i,j}^{0}\right] + \left(\frac{\partial f}{\partial t}\right)_{i,j}^{0} = v_{i,j}^2\left(\psi_{xx} + \psi_{yy}\right)_{i,j} + \left(\frac{\partial f}{\partial t}\right)_{i,j}^{0}, \tag{25}$$

$$\begin{aligned}\left(\frac{\partial^4 u}{\partial t^4}\right)_{i,j}^{0} &= \frac{\partial^2}{\partial t^2}\left(\frac{\partial^2 u}{\partial t^2}\right)_{i,j}^{0} = \frac{\partial^2}{\partial t^2}\left[\left(v^2\left(\frac{\partial^2 u}{\partial x^2} + \frac{\partial^2 u}{\partial y^2}\right) + f\right)_{i,j}^{0}\right] \\ &= v_{i,j}^2\left[\left(\frac{\partial^2 v^2}{\partial x^2} + \frac{\partial^2 v^2}{\partial y^2}\right)_{i,j}\left(\frac{\partial^2 u}{\partial x^2} + \frac{\partial^2 u}{\partial y^2}\right)_{i,j}^{0}\right] \\ &\quad + 2v_{i,j}^2\left[\left(\frac{\partial v^2}{\partial x}\right)_{i,j}\left(\frac{\partial^3 u}{\partial x^3} + \frac{\partial^3 u}{\partial x \partial y^2}\right)_{i,j}^{0}\right. \\ &\quad \left. + \left(\frac{\partial v^2}{\partial y}\right)_{i,j}\left(\frac{\partial^3 u}{\partial y^3} + \frac{\partial^3 u}{\partial y \partial x^2}\right)_{i,j}^{0}\right] \\ &\quad + v_{i,j}^4\left[2\left(\frac{\partial^4 u}{\partial x^2 \partial y^2}\right)_{i,j}^{0} + \left(\frac{\partial^4 u}{\partial x^4} + \frac{\partial^4 u}{\partial y^4}\right)_{i,j}^{0}\right] \\ &\quad + v_{i,j}^2\left(\frac{\partial^2 f}{\partial x^2} + \frac{\partial^2 f}{\partial y^2}\right)_{i,j}^{0} + \left(\frac{\partial^2 f}{\partial t^2}\right)_{i,j}^{0} \\ &= v_{i,j}^2\left[\left(v_{xx}^2 + v_{yy}^2\right)_{i,j}\left(\varphi_{xx} + \varphi_{yy}\right)_{i,j} + 2\left(v_x^2\right)_{i,j}\left(\varphi_{xxx} + \varphi_{xyy}\right)_{i,j}\right. \\ &\quad \left. + 2\left(v_y^2\right)_{i,j}\left(\varphi_{yyy} + \varphi_{xxy}\right)_{i,j}\right] + v_{i,j}^4\left(\varphi_{xxxx} + 2\varphi_{xxyy} + \varphi_{yyyy}\right)_{i,j} \\ &\quad + v_{i,j}^2\left(\frac{\partial^2 f}{\partial x^2} + \frac{\partial^2 f}{\partial y^2}\right)_{i,j}^{0} + \left(\frac{\partial^2 f}{\partial t^2}\right)_{i,j}^{0}.\end{aligned} \tag{26}$$

Substituting Equations (24)–(26) into Equations (21) and (22), respectively, and omitting the truncation error, we obtain

$$\begin{aligned}u_{i,j}^{1/2} &= \varphi_{i,j} + \frac{\tau}{2}\psi_{i,j} + \frac{\tau^2}{8}\left[v_{i,j}^2\left(\varphi_{xx} + \varphi_{yy}\right)_{i,j} + f_{i,j}^{0}\right] \\ &\quad + \frac{\tau^3}{48}\left[v_{i,j}^2\left(\psi_{xx} + \psi_{yy}\right)_{i,j} + \left(\frac{\partial f}{\partial t}\right)_{i,j}^{0}\right] \\ &\quad + \frac{\tau^4}{384}\left[v_{i,j}^2\left(v_{xx}^2 + v_{yy}^2\right)_{i,j}\left(\varphi_{xx} + \varphi_{yy}\right)_{i,j} + v_{i,j}^4\left(\varphi_{xxxx} + \varphi_{yyyy}\right)_{i,j}\right. \\ &\quad \left. + v_{i,j}^2\left(\frac{\partial^2 f}{\partial x^2} + \frac{\partial^2 f}{\partial y^2}\right)_{i,j}^{0} + \left(\frac{\partial^2 f}{\partial t^2}\right)_{i,j}^{0}\right] \\ &\quad + \frac{\tau^4}{192}v_{i,j}^2\left[\left(v_x^2\right)_{i,j}\left(\varphi_{xxx} + \varphi_{xyy}\right)_{i,j}\right. \\ &\quad \left. + \left(v_y^2\right)_{i,j}\left(\varphi_{yyy} + \varphi_{xxy}\right)_{i,j} + v_{i,j}^2\left(\varphi_{xxyy}\right)_{i,j}\right],\end{aligned} \tag{27}$$

$$\begin{aligned}u_{i,j}^{1} &= \varphi_{i,j} + \tau\psi_{i,j} + \frac{\tau^2}{2}\left[v_{i,j}^2\left(\varphi_{xx} + \varphi_{yy}\right)_{i,j} + f_{i,j}^{0}\right] \\ &\quad + \frac{\tau^3}{6}\left[v_{i,j}^2\left(\psi_{xx} + \psi_{yy}\right)_{i,j} + \left(\frac{\partial f}{\partial t}\right)_{i,j}^{0}\right] \\ &\quad + \frac{\tau^4}{24}\left[v_{i,j}^2\left(v_{xx}^2 + v_{yy}^2\right)_{i,j}\left(\varphi_{xx} + \varphi_{yy}\right)_{i,j} + v_{i,j}^4\left(\varphi_{xxxx} + \varphi_{yyyy}\right)_{i,j}\right. \\ &\quad \left. + v_{i,j}^2\left(\frac{\partial^2 f}{\partial x^2} + \frac{\partial^2 f}{\partial y^2}\right)_{i,j}^{0} + \left(\frac{\partial^2 f}{\partial t^2}\right)_{i,j}^{0}\right] \\ &\quad + \frac{\tau^4}{12}v_{i,j}^2\left[\left(v_x^2\right)_{i,j}\left(\varphi_{xxx} + \varphi_{xyy}\right)_{i,j} + \left(v_y^2\right)_{i,j}\left(\varphi_{yyy} + \varphi_{xxy}\right)_{i,j} + v_{i,j}^2\left(\varphi_{xxyy}\right)_{i,j}\right].\end{aligned} \tag{28}$$

Based on the description above, an algorithm for solving Equation (1) by using the EHOC-LOD scheme is given as follows:

Step 1. Let $n = 1$, give the initial time step $u_{i,j}^0$, and the start-up time steps $u_{i,j}^{1/2}$ and $u_{i,j}^1$ are computed by using Equations (27) and (28) $(i, j = 0, 1, \cdots N)$.

Step 2. The values of $(\partial^2 u/\partial x^2)_{i,j}^n$ are computed by Equations (13)–(15) $(i, j = 0, 1, \cdots N)$. Then, the function values $u_{i,j}^{n+1/2}$ are computed by using Equation (12) $(i = 1, \cdots N-1, j = 0, 1, \cdots N)$. The function values $u_{0,j}^{n+1/2}$ and $u_{N,j}^{n+1/2}$ are computed by Equation (3) $(j = 0, 1, \cdots N)$.

Step 3. The values of $(\partial^2 u/\partial y^2)_{i,j}^{n+1/2}$ are computed by Equations (18)–(20) $(i, j = 0, 1, \cdots N)$. Then, the function values $u_{i,j}^{n+1}$ are computed by using Equation (17) $(i = 0, \cdots N, j = 1, \cdots N-1)$. The function values $u_{i,0}^{n+1}$ and $u_{i,N}^{n+1}$ are computed by Equation (3) $(i = 0, 1, \cdots N)$.

Step 4. Let $n \longleftarrow n+1$, repeat Steps 2 and 3 until time reaches the final moment, and the computation is terminated.

3. Stability Analysis

In this section, we analyze the stability of the EHOC-LOD scheme by using the Fourier analysis method.

Lemma 1 (see [33]). *The sufficient and necessary condition for the roots of the quadratic equation $\mu^2 - b\mu - c = 0$ with real coefficients to be not greater than one is $|c| \le 1$, $|b| \le 1 - c$.*

Theorem 1. *The EHOC-LOD scheme in Section 2 is stable if*

$$\max_{1\le i,j\le N}\left|\frac{v_{i,j}\cdot\tau}{h}\right| = v_{\max}\lambda \le 0.8740, \tag{29}$$

in which, $v_{\max} = \max_{1\le i,j\le N}|v_{i,j}|$.

Proof. Let $u_{i,j}^n = \xi^n e^{I\sigma_1 x_i} e^{I\sigma_2 y_j}$, $(u_{xx})_{i,j}^n = \eta^n e^{I\sigma_1 x_i} e^{I\sigma_2 y_j}$, and $(u_{yy})_{i,j}^n = \gamma^n e^{I\sigma_1 x_i} e^{I\sigma_2 y_j}$, where ξ^n, η^n, γ^n are amplitudes, σ_1, σ_2 are phase angles, and $I = \sqrt{-1}$. We assume that $f(x, y, t)$ is exact and does not produce error. Equations (13) and (18) can conclude that

$$\begin{aligned}&\eta^n e^{I\sigma_1 x_i} e^{I\sigma_2 y_j}\left(e^{I\sigma_1 h} + 10 + e^{-I\sigma_1 h}\right)\\ &\quad = \frac{12}{h^2}\xi^n e^{I\sigma_1 x_i} e^{I\sigma_2 y_j}\left(e^{I\sigma_1 h} - 2 + e^{-I\sigma_1 h}\right),\end{aligned} \tag{30}$$

$$\begin{aligned}&\gamma^{n+1/2} e^{I\sigma_1 x_i} e^{I\sigma_2 y_j}\left(e^{I\sigma_2 h} + 10 + e^{-I\sigma_2 h}\right)\\ &\quad = \frac{12}{h^2}\xi^{n+1/2} e^{I\sigma_1 x_i} e^{I\sigma_2 y_j}\left(e^{I\sigma_2 h} - 2 + e^{-I\sigma_2 h}\right).\end{aligned} \tag{31}$$

□

By using Euler's formula, $e^{I\sigma h} = \cos\sigma h + I\sin\sigma h$, $e^{-I\sigma h} = \cos\sigma h - I\sin\sigma h$, Equations (30) and (31) turn to

$$\frac{\eta^n}{\xi^n} = \frac{12(\cos\sigma_1 h - 1)}{h^2(\cos\sigma_1 h + 5)}, \tag{32}$$

$$\frac{\gamma^{n+1/2}}{\xi^{n+1/2}} = \frac{12(\cos\sigma_2 h - 1)}{h^2(\cos\sigma_2 h + 5)}. \tag{33}$$

Let $v_{i,j}^{n+1/2} = u_{i,j}^n$ and $(v_{i,j}^2)_{\max} = a$, and Equation (12) is written in matrix form:

$$\begin{aligned}\begin{bmatrix} u_{i,j}^{n+1/2} \\ v_{i,j}^{n+1/2}\end{bmatrix} &= \begin{bmatrix} 2 & -1 \\ 1 & 0\end{bmatrix}\begin{bmatrix} u_{i,j}^n \\ v_{i,j}^n\end{bmatrix} + \begin{bmatrix} \dfrac{a\tau^2}{2} - \dfrac{a^2\tau^2\lambda^2}{24} & 0 \\ 0 & 0\end{bmatrix}\begin{bmatrix} (u_{xx})_{i,j}^n \\ (v_{xx})_{i,j}^n\end{bmatrix}\\ &\quad + \begin{bmatrix} \dfrac{a^2\tau^2\lambda^2}{48} & 0 \\ 0 & 0\end{bmatrix}\begin{bmatrix} (u_{xx})_{i+1,j}^n \\ (v_{xx})_{i+1,j}^n\end{bmatrix}\\ &\quad + \begin{bmatrix} \dfrac{a^2\tau^2\lambda^2}{48} & 0 \\ 0 & 0\end{bmatrix}\begin{bmatrix} (u_{xx})_{i-1,j}^n \\ (v_{xx})_{i-1,j}^n\end{bmatrix}.\end{aligned} \tag{34}$$

Substituting $(u_{i,j}^n, v_{i,j}^n)^T = \xi^n e^{I\sigma_1 x_i} e^{I\sigma_2 y_j}$, $[(u_{xx})_{i,j}^n, (v_{xx})_{i,j}^n]^T = \eta^n e^{I\sigma_1 x_i} e^{I\sigma_2 y_j}$ into the formula above, we get

$$\begin{aligned}\xi^{n+1/2} &= \begin{bmatrix} 2 & -1 \\ 1 & 0\end{bmatrix}\xi^n + \begin{bmatrix} \dfrac{a\tau^2}{2} - \dfrac{a^2\tau^2\lambda^2}{24} & 0 \\ 0 & 0\end{bmatrix}\eta^n\\ &\quad + \begin{bmatrix} \dfrac{a^2\tau^2\lambda^2}{48}\left(e^{I\sigma_1 h} + e^{-I\sigma_1 h}\right) & 0 \\ 0 & 0\end{bmatrix}\eta^n.\end{aligned} \tag{35}$$

Substituting Equation (32) into Equation (35), we have

$$\begin{aligned}\xi^{n+1/2} &= \begin{bmatrix} 2 & -1 \\ 1 & 0\end{bmatrix}\xi^n + \begin{bmatrix} \dfrac{a\tau^2}{2} + \dfrac{a^2\tau^2\lambda^2(\cos\sigma_1 h - 1)}{24} & 0 \\ 0 & 0\end{bmatrix}\\ &\quad \cdot\frac{12(\cos\sigma_1 h - 1)}{h^2(\cos\sigma_1 h + 5)}\xi^n.\end{aligned} \tag{36}$$

Similarly, Equation (17) can be treated as

$$\xi^{n+1} = \begin{bmatrix} 2 & -1 \\ 1 & 0 \end{bmatrix} \xi^{n+1/2} + \begin{bmatrix} \frac{a\tau^2}{2} + \frac{a^2\tau^2\lambda^2(\cos\sigma_2 h - 1)}{24} & 0 \\ 0 & 0 \end{bmatrix} \cdot \frac{12(\cos\sigma_2 h - 1)}{h^2(\cos\sigma_2 h + 5)} \xi^{n+1/2}. \tag{37}$$

Substituting Equation (36) into Equation (37), the error propagation matrix can be obtained as

$$G = \frac{\xi^{n+1}}{\xi^n} = \begin{bmatrix} B & -1 \\ 1 & 0 \end{bmatrix} \begin{bmatrix} A & -1 \\ 1 & 0 \end{bmatrix} = \begin{bmatrix} BA - 1 & -B \\ A & -1 \end{bmatrix}, \tag{38}$$

where

$$A = 2 + \frac{12a\lambda^2(\cos\sigma_1 h - 1) + a^2\lambda^4(\cos\sigma_1 h - 1)^2}{2(\cos\sigma_1 h + 5)}, \quad B = 2 + \frac{12a\lambda^2(\cos\sigma_2 h - 1) + a^2\lambda^4(\cos\sigma_2 h - 1)^2}{2(\cos\sigma_2 h + 5)}. \tag{39}$$

The characteristic equation can be obtained as

$$|\mu I - G| = \begin{vmatrix} \mu - (BA - 1) & B \\ -A & \mu + 1 \end{vmatrix} = \mu^2 - (AB - 2)\mu + 1 = 0. \tag{40}$$

According to Lemma 1, $|b| = |AB - 2| \le 2$. Due to A and B having the same range of values, we only need to solve $0 \le A \le 2, 0 \le B \le 2$, or $-2 \le A \le 0, -2 \le B \le 0$.

Case 1. When $0 \le A \le 2, 0 \le B \le 2$, we only need to solve $0 \le A \le 2$, i.e.,

$$-4(\cos\sigma_1 h + 5) \le 12a\lambda^2(\cos\sigma_1 h - 1) + a^2\lambda^4(\cos\sigma_1 h - 1)^2 \le 0. \tag{41}$$

Firstly, for the right side of the inequality (41)

$$12a\lambda^2(\cos\sigma_1 h - 1) + a^2\lambda^4(\cos\sigma_1 h - 1)^2 \le 0, \tag{42}$$

we have

$$a\lambda^2 \le 6. \tag{43}$$

Then, for the left side of the inequality (41),

$$-4(\cos\sigma_1 h + 5) \le 12a\lambda^2(\cos\sigma_1 h - 1) + a^2\lambda^4(\cos\sigma_1 h - 1)^2. \tag{44}$$

Letting $\cos\sigma_1 h = \omega, \omega \in [-1, 1]$, the inequality (44) can be expressed as

$$a^2\lambda^4\omega^2 + \left(12a\lambda^2 - 2a^2\lambda^4 + 4\right)\omega + a^2\lambda^4 - 12a\lambda^2 + 20 \ge 0. \tag{45}$$

Letting $F(\omega) = a^2\lambda^4\omega^2 + (12a\lambda^2 - 2a^2\lambda^4 + 4)\omega + a^2\lambda^4 - 12a\lambda^2 + 20$, we assume that $F(\omega)$ is a quadratic function of ω. Then, the function image is a parabola with an upward opening, the axis of symmetry is $-(12a\lambda^2 - 2a^2\lambda^4 + 4)/2a^2\lambda^4$, the ordinate of the vertex is $(-12a^2\lambda^4 - 24a\lambda^2 - 4)/a^2\lambda^4$. In this case, we only need to determine the position of the symmetry axis, so that $F_{\min} \ge 0$ on $\omega \in [-1, 1]$.

Firstly, since $a\lambda^2 \ge 0$, the axis of symmetry $-(12a\lambda^2 - 2a^2\lambda^4 + 4)/2a^2\lambda^4 \le 1$ always holds.

Secondly, when the symmetry axis $-(12a\lambda^2 - 2a^2\lambda^4 + 4)/2a^2\lambda^4 \le -1$, we have $0 \le a\lambda^2 \le (3 + \sqrt{13})/2$. $F(\omega)$ is an increasing function; we only need $F_{\min} = F(-1) \ge 0$, so $a\lambda^2 \le 3 - \sqrt{5}$ or $a\lambda^2 \ge 3 + \sqrt{5}$. But $0 \le a\lambda^2 \le (3 + \sqrt{13})/2$, so $0 \le a\lambda^2 \le 3 - \sqrt{5} \approx 0.7639$.

Finally, when the axis of symmetry $-1 \le -(12a\lambda^2 - 2a^2\lambda^4 + 4)/2a^2\lambda^4 \le 1$, we have $a\lambda^2 \ge (3 + \sqrt{13})/2$. We only need $F_{\min} = F(-(12a\lambda^2 - 2a^2\lambda^4 + 4)/2a^2\lambda^4) \ge 0$, so $(-3 - \sqrt{3})/3 \le a\lambda^2 \le (-3 + \sqrt{3})/3$. But $a\lambda^2 \ge (3 + \sqrt{13})/2 \approx 3.3028$, so there is no solution.

In summary, when $0 \le a\lambda^2 \le 3 - \sqrt{5}$, i.e., $0 \le \sqrt{a}\lambda \le \sqrt{3 - \sqrt{5}} \approx 0.8740$, the EHOC-LOD scheme is stable.

Case 2. When $-2 \le A \le 0, -2 \le B \le 0$, we only need to solve $-2 \le A \le 0$

$$-4 \le \frac{12a\lambda^2(\cos\sigma_1 h - 1) + a^2\lambda^4(\cos\sigma_1 h - 1)^2}{2(\cos\sigma_1 h + 5)} \le -2. \tag{46}$$

Firstly, for the right side of the inequality (46),

$$12a\lambda^2(\cos\sigma_1 h - 1) + a^2\lambda^4(\cos\sigma_1 h - 1)^2 \le -4(\cos\sigma_1 h + 5). \tag{47}$$

According the result of Case 1, we can get that

$$\sqrt{a}\lambda \ge 0.8740. \tag{48}$$

Then, for the left side of the inequality (46),

$$-8(\cos\sigma_1 h + 5) \le 12a\lambda^2(\cos\sigma_1 h - 1) + a^2\lambda^4(\cos\sigma_1 h - 1)^2. \tag{49}$$

Letting $\cos\sigma_1 h = \omega, \omega \in [-1, 1]$, the inequality (49) be expressed as

$$a^2\lambda^4\omega^2 + \left(12a\lambda^2 - 2a^2\lambda^4 + 8\right)\omega + a^2\lambda^4 - 12a\lambda^2 + 40 \ge 0. \tag{50}$$

Letting $G(\omega) = a^2\lambda^4\omega^2 + (12a\lambda^2 - 2a^2\lambda^4 + 8)\omega + a^2\lambda^4 - 12a\lambda^2 + 40$, we assume that $G(\omega)$ is a quadratic function of ω. Then, the function image is a parabola with an upward opening, the axis of symmetry is $-(12a\lambda^2 - 2a^2\lambda^4 + 8)/2a^2\lambda^4$, and the ordinate of the vertex is $(48a^2\lambda^4 - 192a\lambda^2 - 64)/4a^2\lambda^4$. In this case, we only need to determine the position of the symmetry axis, so that $G_{\min} \geq 0$ on $\omega \in [-1, 1]$.

Firstly, since $a\lambda^2 \geq 0$, the axis of symmetry $-(12a\lambda^2 - 2a^2\lambda^4 + 8)/2a^2\lambda^4 \leq 1$ always holds.

Secondly, when the axis of symmetry $-(12a\lambda^2 - 2a^2\lambda^4 + 8)/2a^2\lambda^4 \leq -1$, we have $0 \leq a\lambda^2 \leq (3 + \sqrt{17})/2$. $G(\omega)$ is an increasing function; we only need $G_{\min} = G(-1) \geq 0$, so $0 \leq a\lambda^2 \leq 2$ or $a\lambda^2 \geq 4$. But $0 \leq a\lambda^2 \leq (3 + \sqrt{17})/2 \approx 3.5615$, so $0 \leq a\lambda^2 \leq 2$.

Finally, when the axis of symmetry $-1 \leq -(12a\lambda^2 - 2a^2\lambda^4 + 8)/2a^2\lambda^4 \leq 1$, we have $a\lambda^2 \geq (3 + \sqrt{17})/2$. We only need $G_{\min} = G(-(12a\lambda^2 - 2a^2\lambda^4 + 8)/2a^2\lambda^4) \geq 0$, so $a\lambda^2 \geq (6 + 4\sqrt{3})/3$. But $a\lambda^2 \geq (3 + \sqrt{17})/2$, so $a\lambda^2 \geq (3 + \sqrt{17})/2 \approx 3.5615$.

In summary, due to $(\sqrt{a}\lambda \geq 0.8740) \cap (\sqrt{a}\lambda \leq \sqrt{2}) \cap (\sqrt{a}\lambda \geq \sqrt{3 + \sqrt{17}/2}) = \varnothing$, there is no solution for this case.

Combining Cases 1 and 2, we can conclude that when $\sqrt{a}\lambda = \nu_{\max}\lambda \leq 0.8740$, the EHOC-LOD scheme is stable. This completes the proof.

Table 1 gives the stability conditions of various schemes in Refs. [9–12, 15, 16, 22, 23, 28, 30] and the present EHOC-LOD scheme for the 2D wave equation. Among them, some methods are aimed at the constant wave number wave equation such as Refs. [9, 10, 12, 16, 22, 28, 30]; $|\nu|$ represents the absolute value of the constant wave coefficient. The others deal with the wave equation with variable wave coefficients such as Refs. [11, 15, 23]; $\nu_{\max} = \max_{\alpha \leq x,y \leq \beta} |\nu(x, y)|$ represents the maximum value of the variable wave coefficients. The theoretical analysis result of the stability condition of the EHOC-LOD scheme in this paper is $\nu_{\max}\lambda \in (0,0.8740)$. So, it is more flexible than all the other schemes listed in the literature.

4. Numerical Experiments

This section uses some numerical examples to confirm the accuracy and stability of the proposed EHOC-LOD method. All programs are written in Fortran 90 language by using double-precision arithmetic and run on an Intel Core i5-4210U CPU@1.70 GHz 2.40 GHz desk computer with 4 GB memory.

L_2 and L_∞ norm errors and the rate of convergence are obtained by the following definitions:

$$L_\infty = \max_{0 \leq i,j \leq N} \left| u_{i,j}^M - u\left(x_i, y_j, t_M\right) \right|, L_2 = \sqrt{h^2 \sum_{i,j=0}^{N} \left[u_{i,j}^M - u\left(x_i, y_j, t_M\right) \right]^2},$$

$$\text{Rate} = \frac{\log\left[L_\infty(h_1)/L_\infty(h_2)\right]}{\log\left(h_1/h_2\right)}. \quad (51)$$

Table 1: The stability conditions of various finite difference schemes for solving the 2D wave equations.

Schemes	Stability condition
NACD [10]	$\lvert\nu\rvert\lambda \in (0,0.5080)$
ONAS [30]	$\lvert\nu\rvert\lambda \in (0,0.5629)$
FD [16]	$\lvert\nu\rvert\lambda \in (0,0.7071)$
LOD [28]	$\lvert\nu\rvert\lambda \in (0,0.7321)$
NCPD-ADI [22]	$\lvert\nu\rvert\lambda \in (0,0.8186)$
IRK-DSM [9]	$\lvert\nu\rvert\lambda \in (0,0.8440)$
Mimetic [12]	$\lvert\nu\rvert\lambda \in (0,0.8660)$
FD [15]	$\nu_{\max}\lambda \in (0,0.6124)$
N-TSD-TEM [11]	$\nu_{\max}\lambda \in (0,0.7070)$
NCV-CPD-ADI [23]	$\nu_{\max}\lambda \in (0,0.7321)$
EHOC-LOD	$\nu_{\max}\lambda \in (0,0.8740)$

Table 2: L_2 and L_∞ norm errors when $T = 0.02$ and $\tau = 0.0002$ for Example 1.

h	LOD scheme [28]		EHOC-LOD scheme	
	L_∞	L_2	L_∞	L_2
1/10	3.8515(-6)	1.7507(-6)	1.5824(-7)	7.9120(-8)
1/20	2.4002(-7)	1.1429(-7)	9.8614(-9)	4.9307(-9)
1/40	1.4990(-8)	7.3122(-9)	6.1587(-10)	3.0792(-10)
1/80	9.3644(-10)	4.6244(-10)	3.8498(-11)	1.9238(-11)
1/160	5.8505(-11)	2.9068(-11)	2.4473(-12)	1.2005(-12)
1/320	4.7895(-12)	2.3824(-12)	1.8097(-13)	7.5502(-14)

The CPU time for all the computation is given in seconds.

Example 1 (see [28]).

$$\frac{\partial^2 u}{\partial t^2} = \frac{\partial^2 u}{\partial x^2} + \frac{\partial^2 u}{\partial y^2}, \quad 0 \leq x, y \leq 1, t > 0,$$
$$u(x, y, 0) = \sin(\pi x)\sin(\pi y), \frac{\partial u(x, y, 0)}{\partial t} = 0, \quad (52)$$
$$u(0, y, t) = 0, u(1, y, t) = 0,$$
$$u(x, 0, t) = 0, u(x, 1, t) = 0.$$

The exact solution is

$$u(x, y, t) = \cos\left(\sqrt{2}\pi t\right)\sin(\pi x)\sin(\pi y). \quad (53)$$

Example 1 is a 2D homogeneous wave equation with constant coefficients. Table 2 shows the L_2 and L_∞ norm errors for the EHOC-LOD scheme with $\tau = 0.0002$ and $T = 0.02$. In order to compare, we give the calculated results of the LOD scheme proposed by Zhang et al. in Ref. [28] in Table 2. The results show that the L_∞ and L_2 norm errors

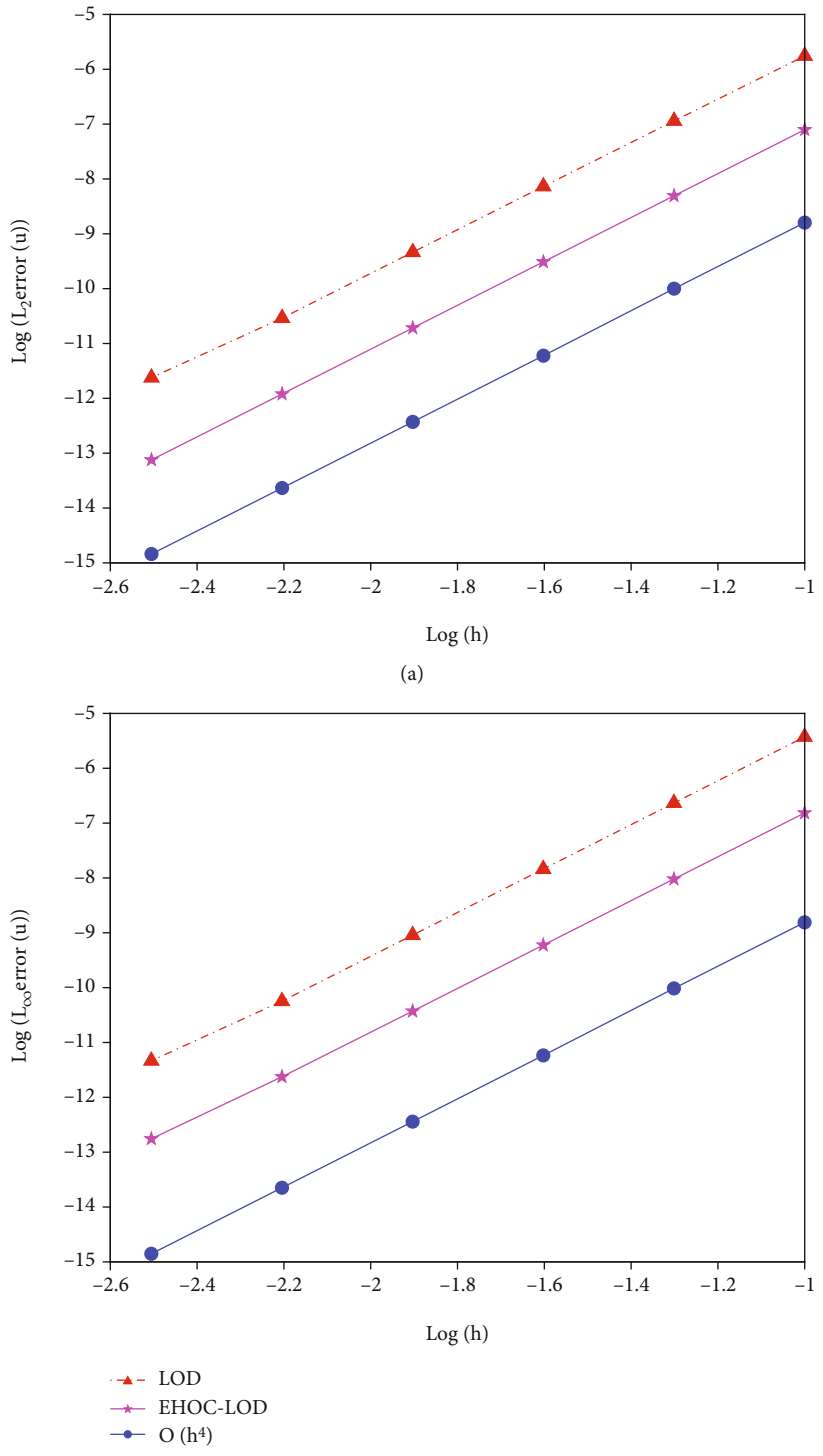

Figure 1: Log-log plots for the L_2 (a) and L_∞ (b) norm errors in space direction.

of the EHOC-LOD scheme are smaller than those of the LOD scheme [28]. In order to verify the computed accuracy of the EHOC-LOD scheme in space direction, in Figure 1, we draw log-log plots for the L_2 and L_∞ norm errors in the space direction for the LOD scheme [28] and the EHOC-LOD scheme. That displays that the slope of the line of the EHOC-LOD scheme is close to 4, which means that the EHOC-LOD scheme can converge with the fourth order in the space direction. When the CFL number is fixed to 0.2 and $T = 0.02$, the L_2 and L_∞ norm errors are listed in Table 3. Obviously, the numerical solution of the EHOC-LOD scheme is a bit better than that of the LOD scheme

Table 3: L_2 and L_∞ norm errors when $T = 0.02$ and the CFL number is fixed at 0.2 for Example 1.

τ	LOD scheme [28]		EHOC-LOD scheme	
	L_∞	L_2	L_∞	L_2
0.0040	5.5715(-8)	2.7858(-8)	5.3806(-8)	2.6903(-8)
0.0025	4.8646(-9)	2.4323(-9)	4.6971(-9)	2.3486(-9)
0.0020	1.3816(-9)	6.9080(-10)	1.3333(-9)	6.6664(-10)
0.0016	3.8135(-10)	1.9071(-10)	3.6722(-10)	1.8363(-10)
0.0010	2.5111(-11)	1.2545(-11)	2.3096(-11)	1.1537(-11)
0.0008	7.5682(-12)	3.7770(-12)	6.1298(-12)	3.0595(-12)

[28]. Then, two log-log plots for the L_2 and L_∞ norm errors in the time direction for the LOD scheme [28] and the EHOC-LOD scheme are shown in Figure 2. Figure 2 shows that the slope of the line of the EHOC-LOD scheme exceeds 4, which means that the EHOC-LOD scheme can converge with the fourth order in the time direction.

Example 2 (see [24]).

$$\frac{\partial^2 u}{\partial t^2} = \frac{\partial^2 u}{\partial x^2} + \frac{\partial^2 u}{\partial y^2} + 3\pi^2 e^{-\pi t} \sin(\pi x + \pi y),$$
$$u(x, y, 0) = \sin(\pi x + \pi y), \frac{\partial u(x, y, 0)}{\partial t} = -\pi \sin(\pi x + \pi y),$$
$$u(0, y, t) = e^{-\pi t} \sin(\pi y), u(1, y, t) = e^{-\pi t} \sin(\pi + \pi y),$$
$$u(x, 0, t) = e^{-\pi t} \sin(\pi x), u(x, 1, t) = e^{-\pi t} \sin(\pi x + \pi). \tag{54}$$

The exact solution is

$$u(x, y, t) = e^{-\pi t} \sin(\pi x + \pi y). \tag{55}$$

Example 2 is a 2D nonhomogeneous wave equation with constant coefficients. In order to make a better comparison, we program the algorithms of the CPR, CDOU, and CSchemeI schemes with second-order accuracy in time and fourth-order accuracy in space in Ref. [24] also in Fortran 90 language. We run the programs on the same computer to make the comparison fair. When $T = 2$, for different spatial grid step length, in Table 4, the L_2 norm errors and CPU time are shown by using the present EHOC-LOD scheme with $\tau = 0.5h$, the CPR, CDOU, and CSchemeI schemes with $\tau = h^2$ in Ref. [24]. We can notice that the EHOC-LOD scheme obtains fourth-order accuracy in both time and space, but those schemes in Ref. [24] must take $\tau = O(h^2)$ to achieve fourth-order accuracy in the space direction. Moreover, the present method gets a more accurate solution. When we define the time as T and the number of grids as N, the total number of time advance steps of the method in this paper is $2NT$, while the total number of time advance steps of those methods in Ref. [24] is N^2T; therefore, the EHOC-LOD scheme expends much less CPU time than those methods in Ref. [24]. With the increase of time T and grid number N, the method in this paper has more significant advantages.

Then, we test the stability condition of the EHOC-LOD method. The L_∞ norm error of the EHOC-LOD scheme with $h = 1/32$ for different T and τ is shown in Table 5. As the time T increases, when $\tau \le 1/37, \nu_{\max}\lambda \le 0.8649$, the EHOC-LOD scheme is convergent. When $\tau \ge 1/36, \nu_{\max}\lambda \ge 0.8889$, the EHOC-LOD scheme is divergent. These computed results are in good agreement with the theoretical analysis.

Example 3 (see [23]).

$$\frac{\partial^2 u}{\partial t^2} = \left[1 + \sin^2(x) + \sin^2(y)\right]\left(\frac{\partial^2 u}{\partial x^2} + \frac{\partial^2 u}{\partial y^2}\right) + \left[3 + 2\sin^2(x) + 2\sin^2(y)\right]e^{-t} \cos(x) \cos(y), 0 \le x, y \le \pi, t > 0,$$
$$u(x, y, 0) = \cos(x) \cos(y), \frac{\partial u(x, y, 0)}{\partial t} = -\cos(x) \cos(y),$$
$$u(0, y, t) = e^{-t} \cos(y), u(\pi, y, t) = -e^{-t} \cos(y),$$
$$u(x, 0, t) = e^{-t} \cos(x), u(x, \pi, t) = -e^{-t} \cos(x). \tag{56}$$

The exact solution is

$$u(x, y, t) = e^{-t} \cos(x) \cos(y). \tag{57}$$

When $T = 1$, for various h and τ, we compute the L_∞ norm error and Rate by using the NCV-CPD-ADI scheme in Ref. [23] and the EHOC-LOD scheme in Table 6. The EHOC-LOD scheme produces the numerical solution with a smaller error than the NCV-CPD-ADI scheme does [23]. In addition, The EHOC-LOD scheme can achieve the fourth-order accuracy in both time and space, while the accuracy of the NCV-CPD-ADI scheme [23] is lower than that of the fourth order.

The stability condition is given by $\nu_{\max}\lambda \le 0.8740$, where $\nu_{\max} = \sqrt{\max_{(x,y)\in[0,\pi]\times[0,\pi]}\left[1 + \sin^2(x) + \sin^2(y)\right]} = \sqrt{3}$ for this example. Therefore, the grid ratio allowed by the EHOC-LOD scheme is $\tau/h \le 0.8740/\sqrt{3} \approx 0.5046$. The grid ratio allowed by the NCV-CPD-ADI scheme [23] is $\tau/h < 0.7321/\sqrt{3} \approx 0.4226$. When we fix $h = \pi/200$, then $\tau < 0.4226\pi/200 \approx 0.00663$ and $1/150 < 0.00663 < 1/151$. We take several numbers near 1/150; Table 7 shows the results. When $\tau \le 1/149$, the L_∞ norm error of the NCV-CPD-ADI scheme [23] and the present scheme are both quite accurate. When $\tau \ge 1/148$, the L_∞ norm error of the NCV-CPD-ADI scheme [23] increases faster, and eventually, it is divergent due to exceeding the stability range. However, the L_∞ norm error of the EHOC-LOD scheme is still quite accurate and convergent. Therefore, the CFL condition of the scheme in this paper is superior to that of the NCV-CPD-ADI scheme [23].

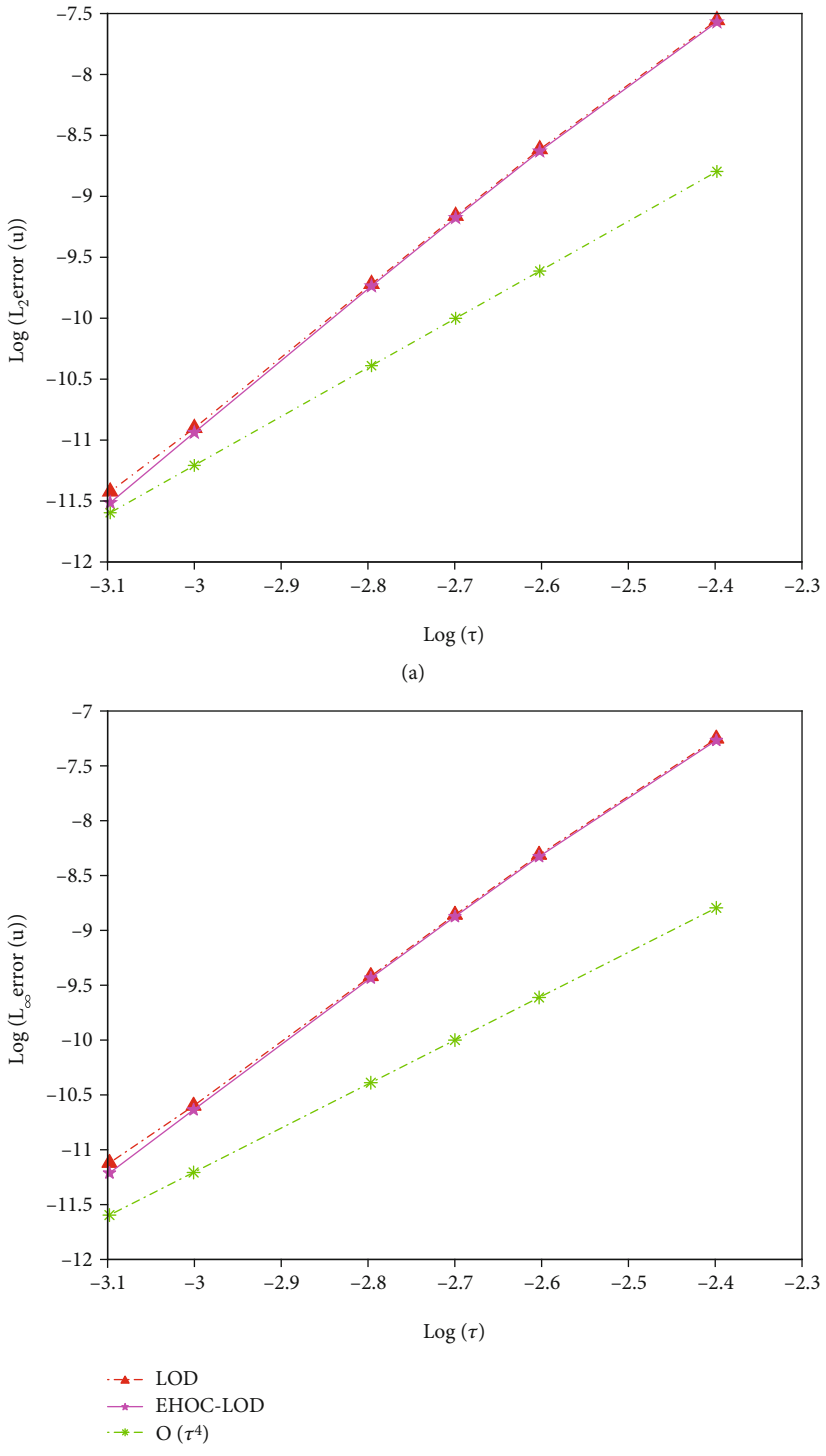

Figure 2: Log-log plots for the L_2 (a) and L_∞ (b) norm errors in time direction.

Table 4: The L_2 norm error and CPU time at $T = 2$ for Example 2.

Schemes	τ	$N = 40$		$N = 60$		$N = 120$	
		L_2	CPU	L_2	CPU	L_2	CPU
CPR [24]	h^2	3.3075(-7)	2.3990	6.5916(-8)	11.8920	1.5789(-9)	200.8900
CDOU [24]	h^2	3.3101(-7)	3.5660	6.5886(-8)	15.6960	1.9432(-9)	218.1560
CSchemeI [24]	h^2	1.0870(-6)	3.6050	2.1494(-7)	17.5510	8.2722(-8)	270.0030
EHOC-LOD	$0.5h$	2.0132(-8)	0.5240	4.1555(-9)	1.6560	2.7109(-10)	13.3130

Table 5: The L_∞ norm error with $h = 1/32$ for different τ and T for Example 2.

τ	$\nu_{\max}\lambda$	$T = 1$	$T = 5$	$T = 10$
1/55	0.5818	2.3265(-8)	5.9423(-8)	4.9813(-8)
1/50	0.6400	1.4417(-8)	5.6307(-8)	1.0922(-7)
1/45	0.7111	4.6947(-8)	7.4385(-8)	1.6359(-7)
1/40	0.8000	1.1738(-7)	1.1719(-7)	3.2546(-7)
1/38	0.8421	1.5834(-7)	1.6067(-7)	3.8232(-7)
1/37	0.8649	1.8287(-7)	1.6693(-7)	4.1226(-7)
1/36	0.8889	1.7126(-5)	3.8468 + 011	8.8343 + 033
1/35	0.9143	3.7430(-2)	5.1554 + 029	4.3232 + 068
1/34	0.9412	3.7129	1.8085 + 040	7.3187 + 089
1/33	0.9697	154.6590	5.2153 + 048	7.3864 + 106

Table 6: L_∞ norm error and Rate when $T = 1$ with various τ and h for Example 3.

(h, τ)	NCV-CPD-ADI [23]		EHOC-LOD	
	L_∞	Rate	L_∞	Rate
$(\pi/40, 1/80)$	2.7242(-6)		2.5481(-8)	
$(\pi/80, 1/160)$	2.2523(-7)	3.5964	1.5691(-9)	4.0298
$(\pi/160, 1/320)$	1.7543(-8)	3.6824	9.7282(-11)	4.0161
$(\pi/320, 1/640)$	1.2928(-9)	3.7623	6.0591(-12)	4.0069

Table 7: The L_∞ norm error with $h = \pi/200$ at $T = 1$ for different τ for Example 3.

τ	NCV-CPD-ADI [23]	EHOC-LOD
1/151	8.1293(-9)	3.7842(-11)
1/150	8.1398(-9)	3.7569(-11)
1/149	8.1505(-9)	3.7639(-11)
1/148	1.2298(-7)	3.7398(-11)
1/147	0.03347	3.7501(-11)

To further verify the stability range of the EHOC-LOD scheme, Table 8 shows the L_∞ norm error of the EHOC-LOD scheme with $h = \pi/200$ for different T and τ. We notice that as time T grows, when $\tau \le 1/127$, $\nu_{\max}\lambda \le 0.8682$, the EHOC-LOD scheme is convergent. When $\tau \ge 1/125$, $\nu_{\max}\lambda \ge 0.8821$, the EHOC-LOD scheme is divergent. The numerical experiment results are consistent with the theoretical ones.

Table 8: The L_∞ norm error with $h = \pi/200$ for different T and τ for Example 3.

τ	$\nu_{\max}\lambda$	$T = 1$	$T = 5$	$T = 10$
1/170	0.6126	3.9454(-11)	2.9495(-11)	7.5373(-12)
1/160	0.6892	3.8399(-11)	2.8656(-11)	6.6731(-12)
1/150	0.7351	3.7968(-11)	2.8299(-11)	6.4342(-12)
1/140	0.7876	3.6524(-11)	2.7555(-11)	6.7108(-12)
1/131	0.8417	3.4756(-11)	2.6059(-11)	7.1994(-12)
1/129	0.8548	3.5237(-11)	2.5741(-11)	7.4449(-12)
1/127	0.8682	3.3824(-11)	2.5329(-11)	7.5574(-12)
1/125	0.8821	3.6304(-11)	8.3126 + 035	2.9323 + 091
1/123	0.8965	2.5429	3.5497 + 075	Overflow

Example 4 (see [23]). Example 4 is a $[0, 5\,\text{km}] \times [0, 5\,\text{km}]$ two-layer model with a wave source. When $y \in (0, 2500\,\text{m})$, the $v(x, y)$ is 1500 m/s; when $y \in (2500\,\text{m}, 5000\,\text{m})$, the $v(x, y)$ is 3000 m/s. Ricker's wavelet source that generates the wave is given by

$$f(x, y, t) = \delta(x - x_0, y - y_0)\left[1 - 2\pi^2 f_p^2 (t - dr)^2\right] e^{-\pi^2 f_p^2 (t-dr)^2}, \tag{58}$$

where $\delta(x - x_0, y - y_0)$ is the Dirac delta distribution, $x_0 = 2500$ m, and $y_0 = 2000$ m. $f_p = 10$ Hz is the peak frequency. $dr = 0.5/f_p$ is the temporal delay that is used to ensure zero initial conditions. The uniform grid size $h = h_x = h_y = 12.5$ m and $\Delta t = 0.001$ s are chosen to solve Example 4.

We draw snapshots of the wave field at different times. Figure 3 describes wave field snapshots computed by the EHOC-LOD scheme: (a) $t = 0.3$ s, (b) $t = 0.65$ s, (c) $t = 0.95$ s, and (d) $t = 1.15$ s. The distance from the source to the rock area is 2500 m-2000 m = 500 m, so when $t = 500\,\text{m}/1500\,\text{m/s} = 0.3333$ s, the wave will reach the rock area. In Figure 3(a), the wave still constitutes a complete circle until it reaches the interface of two layers. As time grows, the wave has reached the rock area; the reflection phenomenon is occurring near the interface, as shown in Figure 3(b). At this time, we can see that the upper and lower parts are two

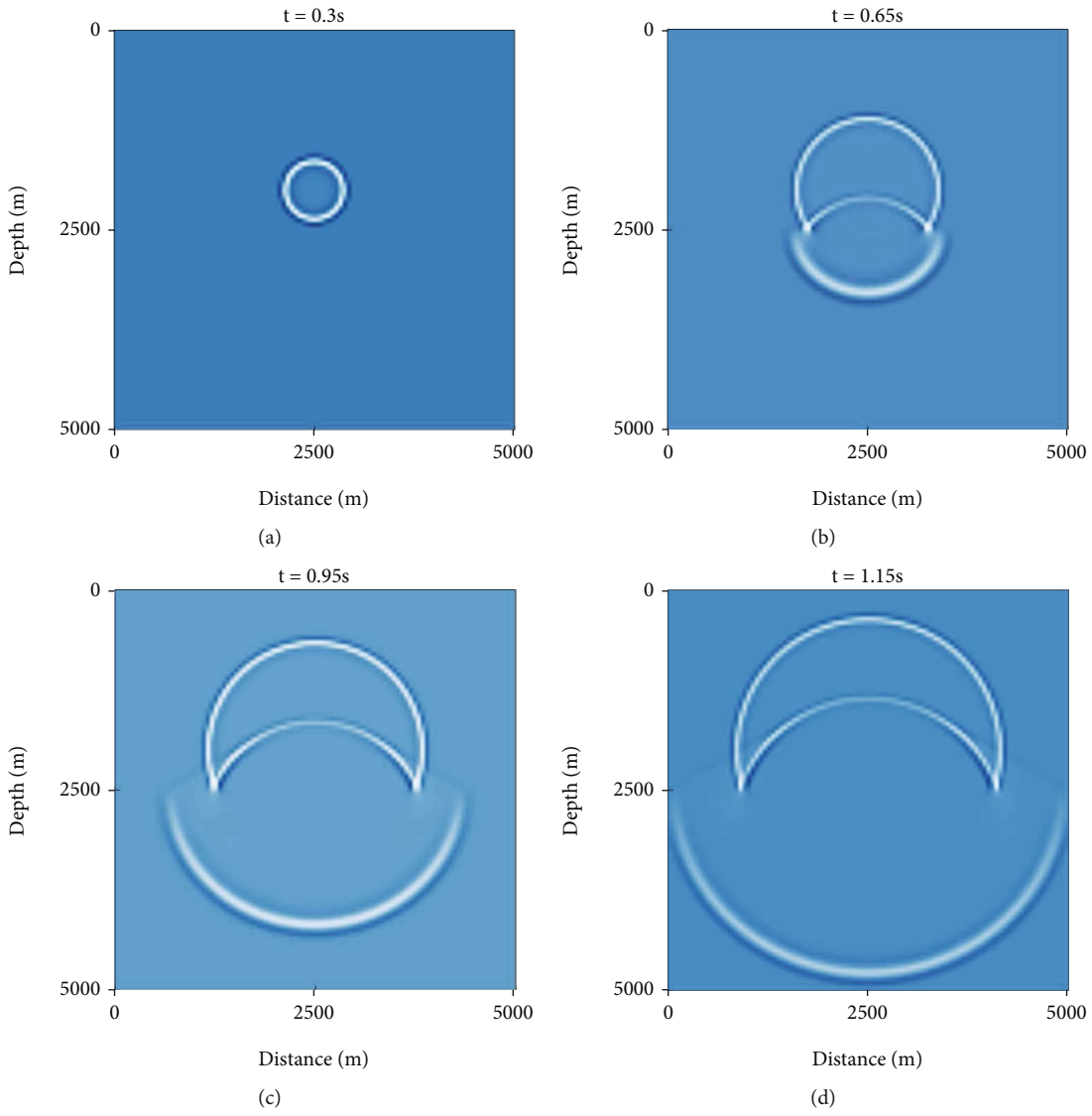

Figure 3: Wavefield snapshots: (a) $t = 0.3$ s; (b) $t = 0.65$ s; (c) $t = 0.95$ s; (d) $t = 1.15$ s.

circles of different sizes, because the wave velocity of the two layers is constant. When the time is 0.95 s, the reflection phenomenon and refraction phenomenon will be further generated, forming a circular wave surface, as shown in Figure 3(c). Finally, in Figure 3(d), the left and right sides of the wave are slightly impacted, resulting in reflection.

5. Conclusions

In this paper, a high accuracy explicit compact difference method for solving the 2D wave equation is presented. Firstly, we use the LOD method to transfer the 2D wave equation into two 1D problems. Then, combined with the fourth-order Padé method, an EHOC-LOD difference scheme is established for the two 1D problems with fourth-order accuracy in both time and space. Afterwards, the stability of the EHOC-LOD scheme is analyzed by the discrete Fourier method, and the range of the stability condition $\nu_{\max}\lambda \in (0,0.8740)$ is obtained. Finally, numerical experiments are conducted to verify the accuracy and stability of the present method. The advantages of this method are mainly reflected in the following aspects:

(i) It can be used not only to compute constant coefficient problems but also to compute variable coefficient problems, even if the wave velocity is discontinuous

(ii) It can be used not only to compute homogeneous problems but also to compute nonhomogeneous problems

(iii) Because of the use of the LOD technique, the computational complexity of the proposed method is significantly reduced. Furthermore, each 1D problem is solved by an explicit computational method, and the computational efficiency is further improved

(iv) The proposed method achieves the fourth-order accuracy; the stability range of the method is the

best among all those schemes of equivalent order of accuracy in the literature

Recently, some authors consider HOC difference schemes for the 3D wave equations [34–36] and the Rosenau-Regularized Long-Wave (RLW) equation [37, 38]. The ADI method was used in Ref. [34, 36] and Mohanty and Gopal [35] proposed an implicit difference scheme. For the 3D Rosenau-RLW equation, Li [37] developed a fourth-order compact and energy-conservative scheme, which is a two-level nonlinear scheme. For the generalized Rosenau-RLW equation, Dimitrienko et al. [38] proposed a conservative fourth-order compact scheme, which is a three-level linear scheme. Generalizing the present EHOC-LOD method to these problems is our ongoing research work. The research results will be reported in the near future.

Data Availability

The data that support this study are available from the corresponding author on reasonable request.

Conflicts of Interest

The authors declare no potential conflict of interests.

Acknowledgments

This work is partially supported by the National Natural Science Foundation of China (12161067, 11772165, 11961054, and 11902170), the National Natural Science Foundation of Ningxia (2022AAC02023 and 2020AAC03059), the Key Research and Development Program of Ningxia (2018BEE03007), the National Youth Top-Notch Talent Support Program of Ningxia, the First Class Discipline Construction Project in Ningxia University: Mathematics, and the Graduate Innovation Program of Ningxia University (2021043).

References

[1] J. Robertsson, J. O. Blanch, K. Nihei, and J. Tromp, *Numerical Modeling of Seismic Wave Propagation: Gridded Two-Way Wave-Equation Methods*, Society of Exploration Geophysicists, 2012.

[2] P. Moczo, J. Kristek, and M. Galis, *The Finite-Difference Modelling of Earthquake Motions: Waves and Ruptures*, Cambridge University Press. Geological Magazine, 2014.

[3] U. Z. Miguel, I. B. Reymundo, and M. U. Jonathan, "High-order implicit staggered-grid finite differences methods for the acoustic wave equation," *Numerical Methods for Partial Differential Equations.*, vol. 34, no. 2, pp. 602–625, 2018.

[4] W. Xu and J. Gao, "Adaptive 9-point frequency-domain finite difference scheme for wavefield modeling of 2D acoustic wave equation," *Journal of Geophysics and Engineering*, vol. 15, no. 4, pp. 1432–1445, 2018.

[5] W. Liang, W. Xiu, Y. Wang, and C. Yang, "A simplified staggered-grid finite-difference scheme and its linear solution for the first-order acoustic wave-equation modeling," *Journal of Computational Physics*, vol. 374, pp. 863–872, 2018.

[6] M. Ran and C. Zhang, "Compact difference scheme for a class of fractional-in-space nonlinear damped wave equations in two space dimensions," *Computers & Mathematics with Applications*, vol. 71, no. 5, pp. 1151–1162, 2016.

[7] Z. Wang, J. Li, B. Wang, Y. Xu, and X. Chen, "A new central compact finite difference scheme with high spectral resolution for acoustic wave equation," *Journal of Computational Physics*, vol. 366, pp. 191–206, 2018.

[8] D. Veiga, L. Beirao, L. Lopez, and G. Vacca, "Mimetic finite difference methods for Hamiltonian wave equations in 2D," *Computers and Mathematics with Applications.*, vol. 74, no. 5, pp. 1123–1141, 2017.

[9] D. Yang, N. Wang, S. Chen, and G. Song, "An explicit method based on the implicit Runge-Kutta algorithm for solving wave equations," *Bulletin of the Seismological Society of America.*, vol. 99, no. 6, pp. 3340–3354, 2009.

[10] D. Yang, P. Tong, and X. Deng, "A central difference method with low numerical dispersion for solving the scalar wave equation," *Geophysical Prospecting*, vol. 60, no. 5, pp. 885–905, 2012.

[11] E. Wang, Y. Liu, and M. Sen, "Effective finite-difference modelling methods with 2D acoustic wave equation using a combination of cross and rhombus stencils," *Geophysical Journal International.*, vol. 206, no. 3, pp. 1933–1958, 2016.

[12] F. Feo, J. M. Jordan, O. Rojas, B. Otero, and R. Rodriguez, "A new mimetic scheme for the acoustic wave equation," *Journal of Computational and Applied Mathematics.*, vol. 295, pp. 2–12, 2016.

[13] E. Wang, J. Ba, and Y. Liu, "Time-space-domain implicit finite-difference methods for modeling acoustic wave equations," *Geophysics*, vol. 83, no. 4, pp. T175–T193, 2018.

[14] Y. Abdulkadir, "Comparison of finite difference schemes for the wave equation based on dispersion," *Journal of Applied Mathematics and Physics*, vol. 3, no. 11, pp. 1544–1562, 2015.

[15] S. Britt, E. Turkel, and S. Tsynkov, "A high order compact time/space finite difference scheme for the wave equation with variable speed of sound," *Journal of Scientific Computing*, vol. 76, no. 2, pp. 777–811, 2018.

[16] Y. Liu and M. Sen, "Time-space domain dispersion-relation-based finite-difference method with arbitrary even-order accuracy for the 2D acoustic wave equation," *Journal of Computational Physics*, vol. 232, no. 1, pp. 327–345, 2013.

[17] A. Portillo, "High-order full discretization for anisotropic wave equations," *Applied Mathematics and Computation*, vol. 323, pp. 1–16, 2018.

[18] C. Chu and P. Stoffa, "Implicit finite-difference simulations of seismic wave propagation," *Geophysics*, vol. 77, no. 2, pp. T57–T67, 2012.

[19] D. W. Peaceman and H. H. Rachford, "The numerical solution of parabolic and elliptic differential equations," *Journal of the Society for Industrial and Applied Mathematics*, vol. 3, no. 1, pp. 28–41, 1955.

[20] J. Douglas and J. E. Gunn, "A general formulation of alternating direction methods," *Numerische Mathematik*, vol. 6, no. 1, pp. 428–453, 1964.

[21] M. Lees, "Alternating direction methods for hyperbolic differential equations," *Journal of the Society for Industrial and Applied Mathematics*, vol. 10, no. 4, pp. 610–616, 1962.

[22] S. Das, W. Liao, and A. Gupta, "An efficient fourth-order low dispersive finite difference scheme for a 2-D acoustic wave equation," *Journal of Computational and Applied Mathematics*, vol. 258, no. 3, pp. 151–167, 2014.

[23] W. Liao, P. Yong, H. Dastour, and J. Huang, "Efficient and accurate numerical simulation of acoustic wave propagation in a 2D heterogeneous media," *Applied Mathematics and Computation*, vol. 321, no. 15, pp. 385–400, 2018.

[24] J. Qin, "The new alternating direction implicit difference methods for the wave equations," *Journal of Computational and Applied Mathematics*, vol. 230, no. 1, pp. 213–223, 2009.

[25] D. Deng, "Unified compact ADI methods for solving nonlinear viscous and nonviscous wave equations," *Chinese Journal of Physics*, vol. 56, no. 6, pp. 2897–2915, 2018.

[26] D. Deng and D. Liang, "The time fourth-order compact ADI methods for solving two-dimensional nonlinear wave equations," *Applied Mathematics and Computation*, vol. 329, no. 15, pp. 188–209, 2018.

[27] A. A. Samarskii, "Local one-dimensional difference schemes for multi-dimensional hyperbolic equations in an arbitrary region," *USSR Computational Mathematics and Mathematical Physics*, vol. 4, no. 4, pp. 21–35, 1964.

[28] W. Zhang, L. Tong, and E. Chung, "A new high accuracy locally one-dimensional scheme for the wave equation," *Journal of Computational and Applied Mathematics*, vol. 236, no. 6, pp. 1343–1353, 2011.

[29] W. Zhang, "A new family of fourth-order locally one-dimensional schemes for the 3D elastic wave equation," *Journal of Computational and Applied Mathematics*, vol. 348, pp. 246–260, 2019.

[30] N. Yun, C. Sun, and C. Sim, "An optimal nearly analytic splitting method for solving 2D acoustic wave equations," *Journal of Applied Geophysics*, vol. 177, article 104029, 2020.

[31] C. Sim, C. Sun, and N. Yun, "A nearly analytic symplectic partitioned Runge–Kutta method based on a locally one-dimensional technique for solving two-dimensional acoustic wave equations," *Geophysical Prospecting*, vol. 68, no. 4, pp. 1253–1269, 2020.

[32] S. K. Lele, "Compact finite difference schemes with spectral-like resolution," *Journal of Computational Physics*, vol. 103, no. 1, pp. 16–42, 1992.

[33] D. Yang, *Iterative Solution for Large Linear System*, Academic Press, New York, 1991.

[34] K. Li, W. Liao, and Y. Lin, "A compact high order alternating direction implicit method for three- dimensional acoustic wave equation with variable coefficient," *Journal of Computational and Applied Mathematics*, vol. 361, pp. 113–129, 2019.

[35] R. K. Mohanty and V. Gopal, "A new off-step high order approximation for the solution of three-space dimensional nonlinear wave equations," *Applied Mathematical Modelling*, vol. 37, no. 5, pp. 2802–2815, 2013.

[36] W. Liao, "On the dispersion, stability and accuracy of a compact higher-order finite difference scheme for 3D acoustic wave equation," *Journal of Computational and Applied Mathematics*, vol. 270, pp. 571–583, 2014.

[37] S. Li, "Numerical analysis for fourth-order compact conservative difference scheme to solve the 3D Rosenau-RLW equation," *Computers & Mathematics with Applications*, vol. 72, no. 9, pp. 2388–2407, 2016.

[38] Y. I. Dimitrienko, S. Li, and Y. Niu, "Study on the dynamics of a nonlinear dispersion model in both 1D and 2D based on the fourth-order compact conservative difference scheme," *Mathematics and Computers in Simulation*, vol. 182, pp. 661–689, 2021.